Hydrologic Response to Land Use Change in a Large Basin in Eastern Amazon

Vanessa Dos Santos, François Laurent, Camila Abe, François Messner

▶ To cite this version:

Article

Hydrologic Response to Land Use Change in a Large Basin in Eastern Amazon

Vanessa Dos Santos [1],* **, François Laurent [1], Camila Abe [2]** **and François Messner [1]**

[1] Laboratoire Espaces et Sociétés (ESO—UMR 6590, ESO CNRS), Le Mans Université, Avenue Olivier Messiaen, 72085 Le Mans CEDEX 9, France; francois.laurent@univ-lemans.fr (F.L.); francois.messner@univ-lemans.fr (F.M.)

[2] National Institute for Space Research (INPE), Av. dos Astronautas 1758, 12227-010 São José dos Campos, Brazil; camilabe@gmail.com

* Correspondence: van.c.dossantos@gmail.com

check for updates

Abstract: Accelerated land use changes in the Brazilian Amazonian region over the last four decades have raised questions about potential consequences for local hydrology. Under the hypothesis of a lack of frontier governance, projections of future changes in the Amazon basin suggest that 20–30% or more of this basin could be deforested in the next 40 years. This could trigger a cascade of negative impacts on water resources. In this study, we examined how a future conversion of the forest into pasture would influence streamflow and water balance components by using a conceptual and semi-distributed hydrological model in a large (142,000 km^2) forested basin: specifically, the Iriri River basin in the Brazilian Amazon. The results showed that the land use change could substantially alter the water balance components of the originally forested basin. For example, an increase of over 57% in pasture areas increased a simulated annual streamflow by ~6.5% and had a significant impact on evapotranspiration, surface runoff, and percolation. Our findings emphasize the importance of protected areas for conservation strategies in the Brazilian Amazonian region.

Keywords: Amazon; land use change; streamflow; water balance components; SWAT model

1. Introduction

Tropical forests have been the focus of scientific and political discussions on surface energy fluxes, hydrological and carbon cycles, vegetation dynamics, land use, and human alteration of the biosphere through agriculture, mining, and urbanization. Land use change (LUC) has aroused significant interest, especially in the largest tropical forest in the world. The Amazon has undergone an accelerated transformation of its forests in the last four decades which has had environmental and socioeconomic impacts [1–9]. The effects of current and future LUC on the hydrology depend on soil–climate–topography–vegetation interactions which vary among basins, and for this reason, these effects remain difficult to predict [1,10,11].

Several studies have analysed different aspects of land use changes in the Brazilian Amazon, including governmental policies to encourage the implementation of agricultural projects, paving roads, population pressure, the commodity market, land speculation, timber exploitation, land tenure conflicts, and lack of public regulation [1,2,4,12–14]. Projections made in 2006 on the future of deforestation in Amazon basin in the absence of frontier governance suggested that 20–30% or more of the basin could be deforested in the next 40 years [8]. However, in practice, since 2006, the deforestation rate has been reduced as a result of the enforcement of laws, commitments by the soy and beef supply chains, restrictions on access to credit, and expansion of protected areas (strictly protected indigenous land and sustainable land use). Between 2005 and 2014, the deforestation rate fell by almost 80%

without slowing the economic growth of the Brazilian Amazon, marking a new stage in the dynamics of land use in this region and revealing better frontier governance [4,15]. Despite the decrease in deforestation since 2006, our analysis is based on the potential change in local hydrology attributable to the serious deforestation scenario built in 2006. This is because law enforcement and supply chain commitments are not yet fully consolidated, as shown by an increase in the deforestation rate at the scale of the Brazilian Amazon in 2015 and 2016 [16].

The use of hydrological models to evaluate changes in hydrologic components is one way to better understand the changes brought about by LUC, to help adapt water resources management, and to provide basis for decision-making or choices related to sustainable development alternatives and conservation practices [17–19]. Numerous studies have used conceptual and semi-distributed hydrological models to evaluate the impact of LUC on hydrology, e.g., Woldesenbet et al. [20], Kamali et al. [21], Zhang et al. [22], Lima et al. [23], and Coe et al. [24]. A recent application in Jamanxim Basin, Pará in the Brazilian Amazon was reported by Lamparter et al. [11]. In general, these studies showed that LUC could trigger a cascade of negative impacts in terms of water balance components (WBC), such as increase in streamflow (Q) and surface runoff (SurfQ) as well as a decrease in evapotranspiration (ET) and infiltration. These impacts can affect the functioning of hydro systems and their uses for navigation, agriculture, energy generation, and directly and/or indirectly affect riverside populations as well as decrease biodiversity conservation.

In this study, we estimated the hydrologic response to LUC in a large basin in the eastern Brazilian Amazon. To this end, we used the 'business-as-usual' (BAU) tropical forest deforestation scenario [8] for 2020, 2030, 2040, and 2050. The BAU scenario represents a lack of frontier governance as was the case before 2006. We chose the BAU scenario for this study to illustrate its impact on streamflow and water balance components. We used the Soil and Water Assessment Tool (SWAT), a conceptual and semi-distributed hydrological model [25–27], to evaluate hydrologic responses to LUC.

2. Study Area

The Iriri River Basin is located at the eastern region of the Amazon Basin (Figure 1), between the Brazilian states of Mato Grosso (headstreams) and Pará, and is one of the main tributaries of the left bank of the Xingu River. The total length of the Iriri River is approximately 1,300 km and the total area of the Iriri River basin is 142,000 km^2. About 80% of the basin, which comprises eleven indigenous territories and seven protected areas, is legally protected from deforestation.

The Iriri River basin is situated in a climatic transition region between the tropical monsoon climate (Am) in the north and tropical savanna climate (Aw) in the south, according to the Köppen classification. The main atmospheric systems responsible for climatic dynamics in this region are the Intertropical Convergence Zone and the South Atlantic convergence zone. Due to a south–north gradient, the annual average precipitation rate is 1800 mm per year, ranging from 1500 to 2500 mm per year. Seasonality is well-defined, with a rainy season lasting from December to June and a dry season from July to November. Relative air humidity is above 80% almost every month of the year. The average temperature ranges between 24 °C and 28 °C. Minimum temperatures rarely fall below 16 °C and mean maximum temperatures range between 33 °C and 36 °C, with the highest values generally occurring between August and March (Figure 1B) [28–30].

The area is formed by Precambrian crystalline complexes and meta-volcano-sedimentary rocks as well as Pleistocene sediments. In general, this type of lithology is dominated by fractured aquifers covered by weathered mantles (soils and altered rocks) of variable thickness. The predominant soil in the basin is yellow Acrisol which occupies approximately 86% of the total area [28].

The vegetation in the Iriri River basin is characterized by continuous forest (approximately 90% of the total area [31]) formed by open ombrophilous forests (moist tropical rainforest) and climatic gradients with more than 60 dry days as well as dense ombrophilous forests with dry periods lasting for less than 60 days. Enclaves of savanna (*cerrado*) are associated with ombrophilous forest [32]. In 2014, pastures accounted for 3.2% of the basin [31].
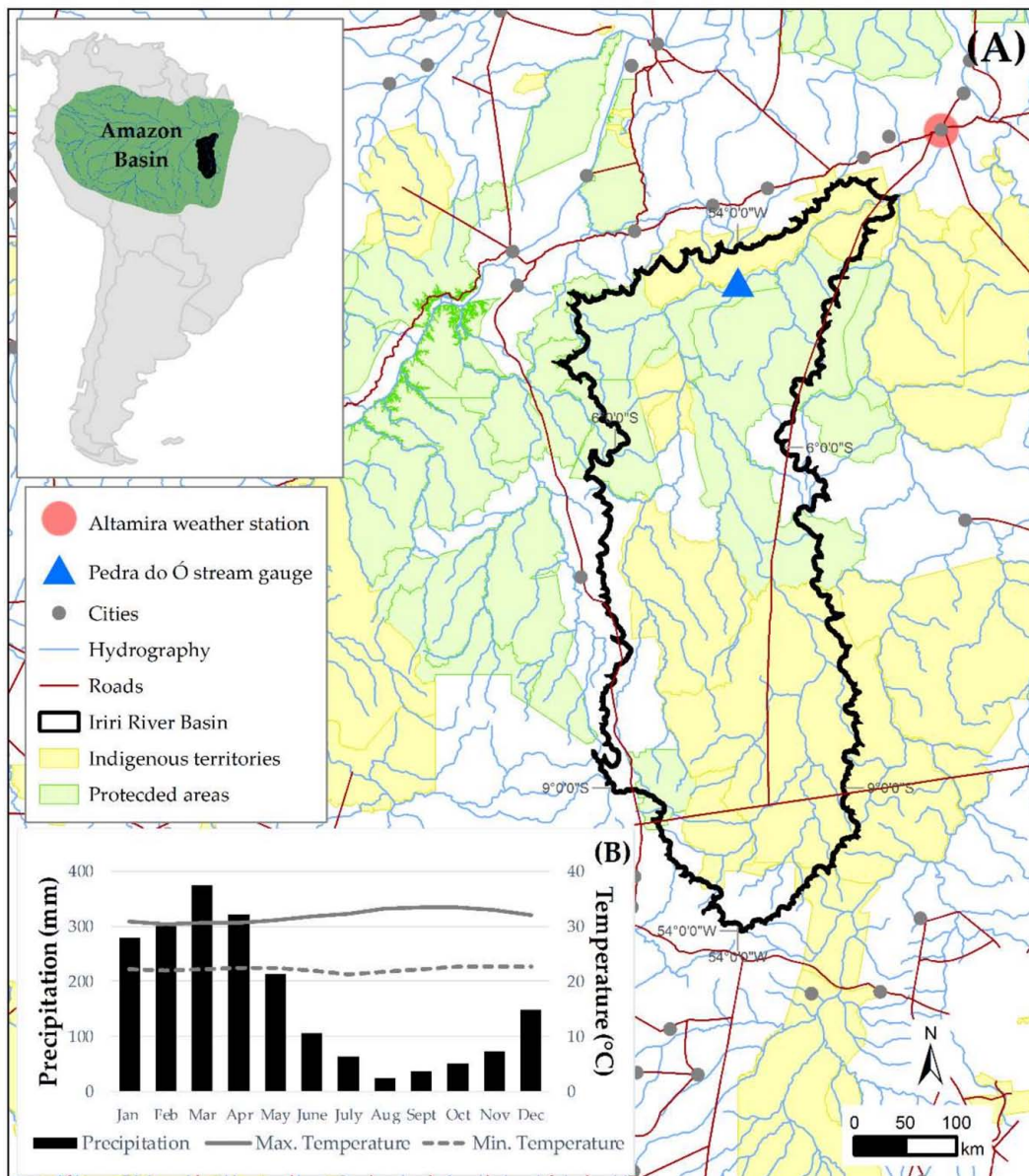
Figure 1. Study area. (**A**) Iriri River Basin and location of indigenous territories and protected areas; (**B**) Precipitation and temperature regimes on Altamira weather station.

3. Materials and Methods

3.1. The Model and the Simulation Design

3.1.1. Description of the SWAT Model

The SWAT model was designed to predict the impact of land use and management on water, sediment, and agricultural chemical yields at catchment scale at daily, monthly, and annual time increments. In SWAT, the basin is divided into sub-basins comprising a river segment and hydrological response units (HRUs), which represent areas of homogeneous land use, topography, and soil characteristics [25–27].

By modeling the hydrological cycle, SWAT computes the amount of water in the streams and in the soil as well as the fluxes of surface runoff (SurfQ), evapotranspiration (ET), and the amount of water stored in shallow and deep aquifers. The model also determines sediment, nutrient, and pesticide

yields via routing processes to describe the movement of water, sediments, and other components through the channel network of the basin to the outlet [27,33]. In this study, we focused on the hydrological processes to predict streamflow (Q), SurfQ, ET, and groundwater. The simulations of these components are based on the water balance given in Equation (1) [25]:

$$SW_t = SW_0 + \sum_{i=1}^{t} \left(R_{day\ i} - Q_{surf\ i} - E_{a\ i} - w_{seep\ i} - Q_{gw\ i} \right) \tag{1}$$

where SW_t is the final soil water content (mm H_2O); SW_0 is the initial soil water content (mm H_2O); t is time (days); R_{dayi} is precipitation on day i (mm H_2O); Q_{surfi} is surface runoff on day i (mm H_2O); E_{ai} is evapotranspiration on day i (mm H_2O); w_{seepi} is the amount of water from the soil profile inflowing to the vadose zone on day i (mm H_2O); and Q_{gwi} is the base flow on day i (mm H_2O).

3.1.2. Model Input Data

The main input data used to characterize the basin, soil types, land cover, topography (Figure 2), and climate (temperature and precipitation) are spatialized over the basin. To fulfill this requirement, the main input data in the model in this study include remote sensing and reanalysis products (Table 1).
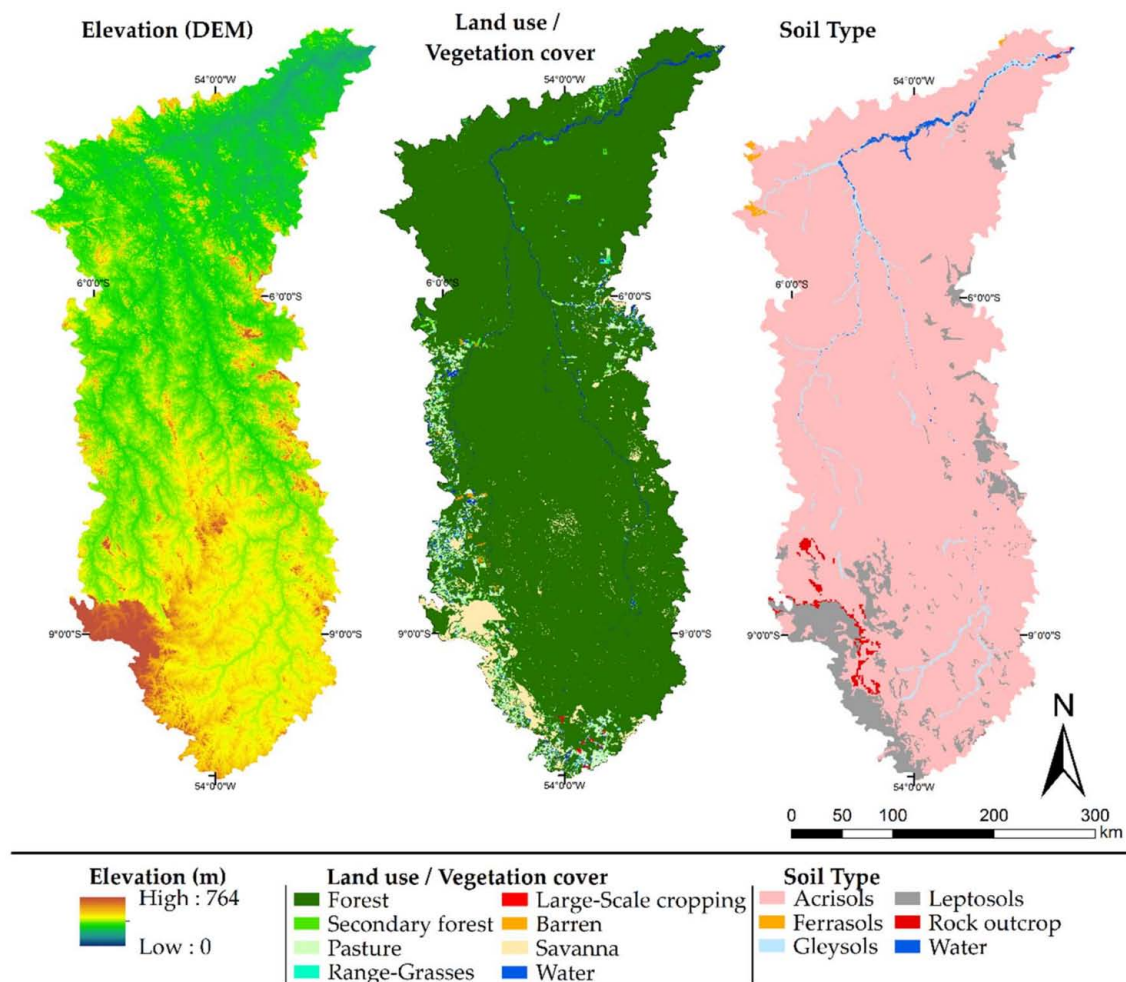

Figure 2. The Digital Elevation Model, land cover, and soil types in the Iriri River Basin.

Table 1. Main model input data.

Input Data	Source	Description (Time Series)
Digital Elevation Model (DEM)	Shuttle Radar Topography Mission [34]	SRTM 3 arc-seconds for global coverage—~90 m
Weather	Brazilian Meteorological Service [35]	Daily precipitation, daily temperature (min., max.), solar radiation, relative air humidity, wind speed (1970–2015)
Precipitation	TRMM product 3B42 V.7 Daily product [36]	Daily TRMM precipitation estimates for a 0.25° grid (1998–2015)
Temperature	ERA Interim Daily Product [37]	Daily Temperature for a 1° grid (1998–2015)
Land Use/vegetation cover	TerraClass project [31] and database from literature	Land use/vegetation cover map 1:250,000 and specific vegetation parameters
Soil	Soil map [38] and pedotransfer functions	Soil map 1:250,000 and specific soil properties for each soil type

- Weather Data

The European Reanalysis (ERA) Interim temperature estimate dataset was cross-referenced with *in situ* data from the Altamira weather station (Figure 1A). When compared with *in situ* data, it was found that, on average, the ERA Interim minimum temperatures dataset was systematically overestimated by 1.53 °C, whereas the maximum temperature dataset was underestimated by 6.74 °C. Therefore, a linear bias correction was applied to the ERA Interim dataset by summing −1.53 °C and +6.74 °C to the minimum and maximum ERA Interim temperatures, respectively. In this study, TRMM 3B42 V.7 Daily product precipitation estimates was the forcing variable of the model, and the data series used (daily precipitation rates from 1998 to 2015) were validated for the Xingu Basin region by cross-referencing the dataset with *in situ* P gauge (Altamira weather station). This validation resulted in an R^2 of 0.76 and Relative Root Mean Square Error—% (RMSE) of 31%, indicating that TRMM 3B42 V.7 can be used to represent the P rates in the Iriri River basin for modeling purposes.

- Land Use/Vegetation Cover

Parameters regarding the physical and physiological characteristics of the vegetation were required to model the interactions between vegetation and water, especially the ET process. SWAT has a database with recommended vegetation parameter values for several vegetation types and crops. These include three types of forests: evergreen, deciduous, and mixed forests. However, the 'SWAT vegetation database was developed for temperate zones and was not suitable for tropical climates [39–41].

Tropical evergreen forest, which is the predominant vegetation in the Iriri River basin, shows a high spatial variability in canopy properties that affects ET across the region. Furthermore, forest activity (phenology and productivity) in the Amazonian region is mainly controlled by solar radiation (leaf flushing usually coincides with periods of increased radiation) [42,43] and soil water availability (the forest continues to grow even during the dry season, since its deep root system is able to reach water stored in deep soil layers, and there is more radiation available in the dry season because of less cloud cover) [42,44–47]. Therefore, we adapted the SWAT database (evergreen forest, pasture, and savanna) to tropical conditions using a combination of parameter values found in the literature [48–50].

- Soil

Some soil characteristics, including porosity and available water capacity, are crucial for computing soil water content and hence the water balance. The SWAT soil database was developed for soils in temperate climate areas and its parameter values are consequently not representative of tropical soils. Therefore, the soil data and parameters were adapted for this study.

The Amazonian region encompasses a wide variety of different soil types that reflect the diversity of geologic origins and weathering processes. In general, the soils are highly weathered, deep, clayey, and porous [51,52]. Using mean texture values from the literature [52–58], the main soil parameters such as bulk density, available water capacity, and saturated hydraulic conductivity were estimated using pedotransfer functions developed for Amazonian soils [51,59–62].

3.1.3. Model Setup

SWAT2012 version [63] was set up for the Iriri River basin using the input data listed in Table 1. The basin was divided into 18 sub-basins, delineated by stream confluences defined using the Digital Elevation Model (DEM). The 18 sub-basins were then divided into 407 HRUs, representing homogenous land use, soil, and slope classes.

The study area lacked several elements of meteorological data. Therefore, the Hargreaves method was used to estimate potential ET [64] because, among the methods available in SWAT, this requires fewer meteorological data. Thus, this choice was also an attempt to avoid the introduction of more uncertainties into the model, which potentially may have arisen from estimating more meteorological data. The surface runoff (SurfQ) was calculated using the Soil Conservation Service's Curve Number method [65] and the Muskingum method was used for channel routing [66].

The model simulation covered a total period of 17 years (1998–2015), with shorter series used for model warm-up (1998–2000), calibration (2001–2009), and validation (2010–2012) as described below. To predict the impact of future developments in the basin, a future scenario was used for simulations of four different years: 2020, 2030, 2040, and 2050.

We used the Land Use Update Tool [67] to update land use distribution by updating the HRU fractions during the model run.

3.1.4. Calibration and Validation

Model calibration was based on the optimization of the parameter values by adjusting the simulated streamflow (Q_{sim}) at the outlet of the basin with observed streamflow (Q_{obs}). The monthly Q_{obs} data from the gauge Pedra do Ó (station 18700000, with a basin area of 123,827 km^2) (Figure 1A) was available for the period 1999–2012 (ANA—Brazilian National Water Agency). In this study, the parameters related to ET, groundwater, and Q were initially adjusted by manual calibration (trial and error). The Parameter Solution (ParaSol) [68] implemented in the SWAT-CUP software package [69] was used for sensitivity analysis, model calibration, and uncertainty analysis. The ParaSol method aggregates objective function (OF), which is calculated based on the model outputs and on the observed data, into a global optimization criterion (GOC). Then, the algorithm minimizes these OF's or a GOC using the Shuffle Complex Evolution algorithm (SCE-UA) and performs an uncertainty analysis with a choice between two statistical concepts. This algorithm uses the sum of squares of the residuals (SSQ) as an objective function and the Nash-Sutcliffe Efficiency (NSE [70]) as a goal function to determine the best parameter values [68,71].

Validation was performed using Q_{obs} dataset that was not used for calibration, and model performance was assessed using the periods of calibration (2001–2009), validation (2010–2012), and the whole series (2001–2015) using the coefficient of determination (R^2), the NSE, the Percent Bias (PBIAS) [72], and the Root Mean Squared Error Observations Standard Deviation Ratio (RSR) [73].

3.2. Land Use Scenario

We used the 'business-as-usual' (BAU) scenario developed by Soares-Filho et al. [8] through an application of the SimAmazonia model. This model compares the potential influence of protected areas and other conservation approaches on future trends in the Amazon basin to vegetation types, using an empirically-based, policy-sensitive model of Amazon deforestation. The SimAmazonia model simulates monthly deforestation in the Amazon Basin from 2002 to 2050 and includes eight scenarios that encompass a plausible range of future deforestation trajectories.

BAU is an extreme scenario that predicts deforestation using historical images (PRODES data [16]) and their variations between 1997 and 2002 as well as adding the effect of paving a set of major roads. The BAU scenario assumes the deforestation trends that occurred across the Amazon basin up to 2006 will continue in the future, i.e., that highways scheduled for paving at the beginning of the 2000s will be paved, compliance with legislation requiring forest reserves on private land will remain low (like at the beginning of 2000s), and no new protected areas will be created. The BAU scenario also assumes that 40% of the forests inside protected areas and 85% outside protected areas will be subject to deforestation [8,74].

The BAU scenario presents three patterns of land use: "deforested", i.e., the removal of native forest; "forest", i.e., the native forest; and "non-forest", i.e., other types of native vegetation (e.g., savanna). In SWAT, deforested areas were set as pasture. Indeed, pastures for livestock farming occupy approximately 60% of the total deforested areas throughout the Brazilian Amazon [31]. "Forest" was set as "evergreen forest" and "non-forest" areas corresponded to "savanna" areas in the Iriri River basin. Savanna areas represent 2.51% of total area in the basin and this percentage has remained unchanged over the years. Figure 3 gives an overview of the future LUC scenario in the Iriri River basin for the years 2020, 2030, 2040, and 2050.
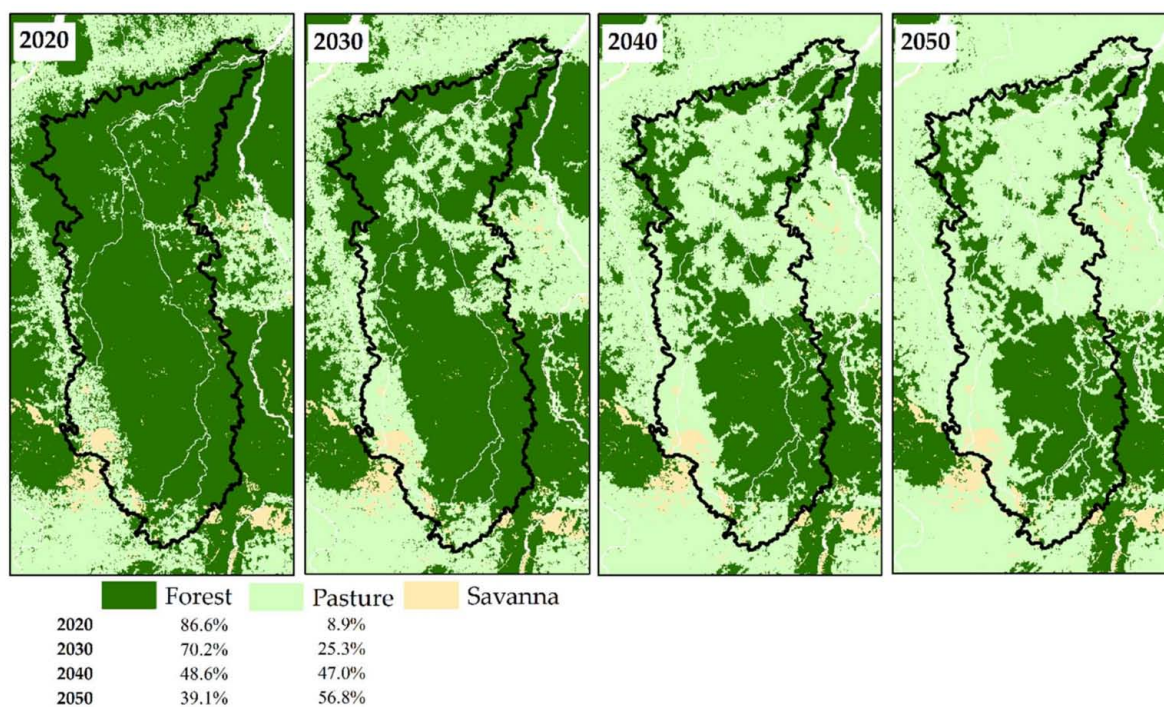

	Forest	Pasture
2020	86.6%	8.9%
2030	70.2%	25.3%
2040	48.6%	47.0%
2050	39.1%	56.8%

Figure 3. 'Business-as-usual' scenario for 2020, 2030, 2040, and 2050 in Iriri River Basin [8,73].

4. Results

4.1. Model Calibration and Efficiency

4.1.1. Model Calibration

Model calibration was divided into two stages: manual and automatic calibration. Parameters were manually calibrated to adjust the evapotranspiration (ET) rates and leaf area index (LAI) curve. The LAI curve for evergreen forest, pasture, and savanna were adjusted thereby changing the SWAT vegetation parameters that determine the shape of the LAI curve to match observations [40,43,75,76]. This reported LAIs with annual averages of 4.02 m^2/m^2 for evergreen forest, 1.09 m^2/m^2 for pasture, and 1.25 m^2/m^2 for savanna. The ET was determined by changing SWAT vegetation, soil, and groundwater parameters

and led to an annual average ET rate of 56% of the annual average precipitation, corresponding to the rates reported for the eastern Amazon [44,47,77,78] and to data from the Altamira weather station (Figure 1A).

Global sensitivity analysis was performed using 14 parameters related to channel, groundwater, and runoff, resulting in eight parameters ranked as significantly sensitive (p-value < 0.05). These parameters were then included in the automatic calibration procedure. The sensitivity rank of the parameters and the results of the automatic calibration are shown in Table 2.

Table 2. SWAT parameters modified in the automatic calibration phase.

Parameter [Land Use/ Vegetation Cover]	Parameter Description [Model File]	Sensitivity Ranking	Initial Range	Final Calibrated Range	Best Calibrated Value	Degree (%) of Uncertainty **
*v__CN2 [b] [Evergreen Forest]	Initial SCS runoff curve number for moisture condition II [*.mgt]	2	20–82	23–64	32	66.13
*v__CN2 [b] [Pasture]		3	35–82	52–72	66	42.55
*v__CH_K2 [a]	Effective hydraulic conductivity in main channel alluvium (mm h^{-1}) [*.rte]	8	0–150	49–82	63	22
*v__CH_N2 [a]	Manning's "n" value for the main channel [*.rte]	5	0.1–0.3	0.03–0.09	0.078	30
*v__GW_DELAY [Evergreen Forest]	Groundwater delay time (days) [*.gw]	7	0–200	10–55	29	22.5
*v__GW_DELAY [Pasture]		6	0–200	63–115	92	26
*v__GWQMN [Evergreen Forest]	Threshold depth of water in the shallow aquifer required for return flow to occur (mm H_2O) [*.gw]	1	0–1000	30–147	103	11.7
*v__GWQMN [Pasture]		4	0–1000	41–156	130	11.5

*v__ Value, calibration is performed by replacing the initial value; ** The degree of uncertainty is the ratio between final calibrated range multiplied by 100 and the initial range; [a] Non-specific for land use/vegetation cover; [b] Depends on the land use/vegetation cover and soil type.

Calibration reduced CN2 values for tropical evergreen forest when compared with pasture, confirming the expected high infiltration in forested areas [79–81]. The CH_N2 calibrated value represents natural streams with heavy timber and brush [82], which is expected for reaches in forested areas like the Iriri River basin. For parameter CH_K2, the calibrated value (63 mm h^{-1}) indicates that the river bed material is mainly a mixture of sand and gravel with low silt-clay content [83]. This is reasonable and agrees with the classification of streams in the eastern Amazon Basin as clear-water rivers with little suspended sediment [84]. The values calibrated for the parameters related to groundwater (GW_DELAY and GWQMN) are coherent because the Iriri River basin is part of the Brazilian shield, which usually implies deep thin aquifers with low yields [85]. The difference between evergreen forest and pasture groundwater parameters can be explained by faster lateral runoff from pasture than that from forest.

4.1.2. Efficiency

As shown in Figure 4A, the resulting simulated monthly streamflow (Q_{sim}), using the best set of calibrated parameter values, reproduced the observed streamflow (Q), as confirmed by efficiency criteria (Table 3) and by the percentage prediction uncertainty (95PPU is calculated at the 2.5% and 97.5% levels of the cumulative distribution of an output variable obtained through Latin hypercube sampling [69]).
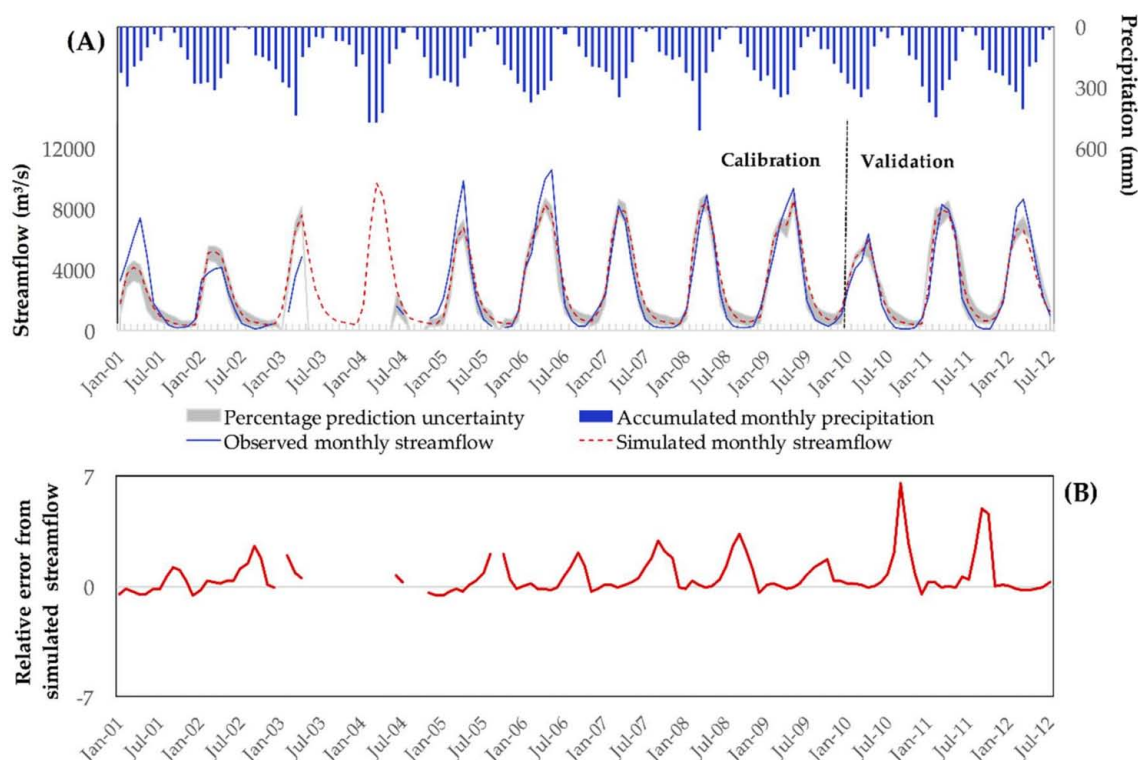
Figure 4. (**A**) Monthly simulated and observed streamflow, and the precipitation data used for the calibration and validation periods, and (**B**) relative error between monthly average streamflow (Relative error = $(Q_{sim} - Q_{obs})/Q_{obs}$).

Table 3. Coefficients used to assess the model performance during the calibration, validation and entire period, and the classification of model performance, according to Moriasi et al. [86].

Coefficient	Calibration Period	Validation Period	Entire Series	Classification for Entire Series
R^2	0.86	0.95	0.88	-
NSE	0.85	0.94	0.87	Very good
RSR	0.38	0.25	0.36	Very good
PBIAS (%)	−7.47	−3.2	−6.36	Very good

The resulting 95PPU was narrow and did not cover most of the extreme high and low flow periods, corresponding to a P-factor (percentage of observations covered by the 95PPU) and R-factor (average thickness of the 95PPU band divided by the standard deviation of the measured) of 0.64 and 0.58 respectively for the entire series.

Figure 4B shows the relative error between Q_{obs} and Q_{sim} (positive values indicate overestimated Q_{sim} and negative values indicate underestimated Q_{sim}). For some episodes in the calibration and validation periods, Q_{sim} was slightly underestimated during peak flow, compared with observed streamflow (Q_{obs}). Inversely, the model overestimated minimum values of Q_{obs}. In reality, the recession was faster and the baseflow during the dry season was lower. This error could not be corrected by an increase of baseflow recession constant (ALPHA_BF parameter) because it would lead to overestimating streamflow during the beginning of the rainy season (October to January). The higher relative errors for 2010 and 2011 dry seasons are explained by the very low values of streamflow during these years of strong dryness, with a monthly mean of 73 and 111 $m^3 \cdot s^{-1}$, respectively for September 2010 and September 2011, which is largely beneath the mean of 201 $m^3 \cdot s^{-1}$ for September months of the period.

4.1.3. Water Balance Components at the Scale of the Hydrological Response Units

To better understand the influence of land use in water balance components (WBC), we analyzed average annual ET, surface runoff (SurfQ), and Percolation (Perc) simulated at the HRU scale for forest and pasture in Acrisol (which represents ~86% of the total area of the Iriri River basin). The results showed that ET and Perc are higher in forest HRU (>3% per year and >4% per year, respectively) than in pasture HRU, on the other hand, SurfQ is higher in HRU represented by pasture (>7% per year) (Figure 5). This is in agreement with other studies showing that ET and Perc are lower and SurfQ is higher in pasturelands [78,87–90].
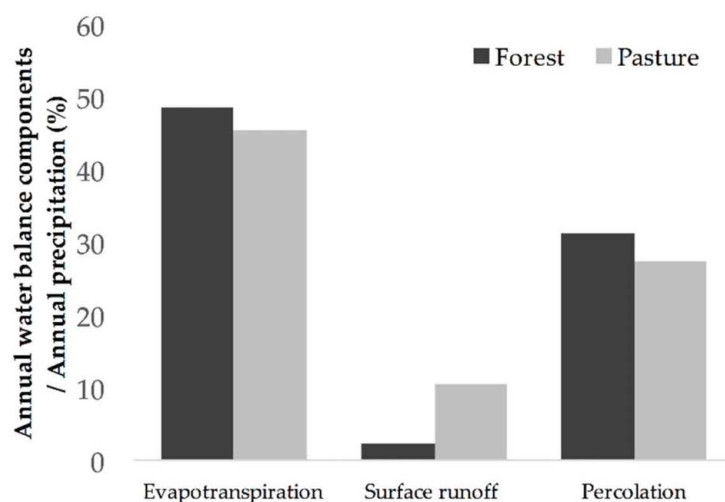

Figure 5. Components of the annual water balance in relation to average annual precipitation at the scale of hydrological response units.

4.2. Scenario Application

The LUC scenarios were run using identical weather data (the 17-year data series) so that variations in Q and other WBC were solely attributable to LUC. The LUC increased the annual average Q from 0.3% to 6.5% between 2020 and 2050, compared with the baseline Q (Q was simulated using land use in 2014 based on data from the TerraClass Project [31]) (Table 4).

Table 4. Percent difference between annual average water balance components simulated for 2020, 2030, 2040, and 2050 and simulated in the baseline scenario.

Base Scenario	Q (mm)	ET (mm)	SurfQ (mm)	Perc (mm)
2014	862	1161	70	609
Scenario	**pQ (%)**	**pET (%)**	**pSurfQ (%)**	**pPerc (%)**
2020	0.3	−0.1	6.6	−0.1
2030	1.8	−1.9	51.1	−7.2
2040	5.1	−6.6	119.8	−16.5
2050	6.5	−10.6	183.1	−21.9

The mean percentage difference [p(%)] is calculated using each Water Balance Component dataset as reference (pWBC = baseline − WBC).

The monthly average Q of the baseline and of the future scenarios are presented in Figure 6A. During the first part of the recession phase, from the peak flow to the end of the rainy season (March to June), the simulated Q was slightly lower than baseline values, particularly in 2040 and 2050 when the area under pasture has been extended. Inversely, in the remaining year period, the expansion of pasture across the scenarios caused an increase in Q, particularly at the beginning of the rainy season,

from October to January. The percent differences (Figure 6B) showed that even a slight change in land cover (2020: pasture expands from 3.2% to 8.9% of the total basin area) is sufficient to increase Q by up to 8% during the rising water phase in December. The consequence of deforestation for Q was even more dramatic in 2040 and 2050, with a maximum increase of 99% in December and a decrease during low Q with a reduction of up to 8% in April.
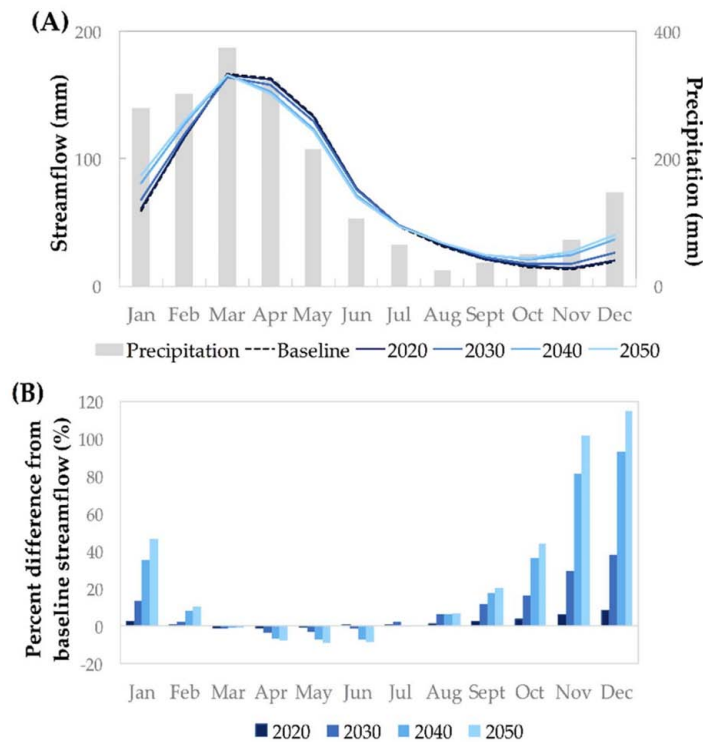

Figure 6. (**A**) Monthly average simulated streamflow and (**B**) percent differences between monthly average streamflow simulated for 2020, 2030, 2040, 2050, and that simulated for baseline.

LUC also had a marked impact on other WBC at basin scale. At yearly scale, ET decreased from −0.1 to −10.6% between 2020 and 2050 (Table 4). ET decreased sharply during the dry season with a 10 to 20% reduction from June to October (Figure 7), caused by the reduction in pasture ET compared with forest ET as a result of higher stomatal leaf resistance and shallower grass roots. The variation was greater for 2040 and 2050 with the major expansion of pasture.
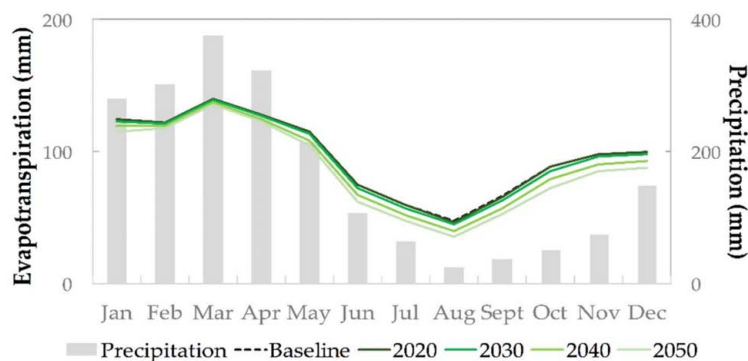

Figure 7. Monthly average simulated evapotranspiration for 2020, 2030, 2040, 2050, and the baseline.

The increase of SurfQ in pasture, compared with forest, was caused by lower vegetation cover and higher soil compaction by grazing cattle, which was represented by the Soil Conservation Service's

Curve Number (CN) in the SWAT model. At yearly scale, the SurfQ increased drastically from 6.6% in 2020 to 183.1%, in 2050 (Table 4). The monthly SurfQ dynamics depended on the precipitation (Figure 8). SurfQ remained negligible from June to October (<5 mm/month). The increase in SurfQ caused by deforestation was higher during the rainy season with a maximum in March (+26 mm, equivalent to a 158% an increase compared to the baseline).
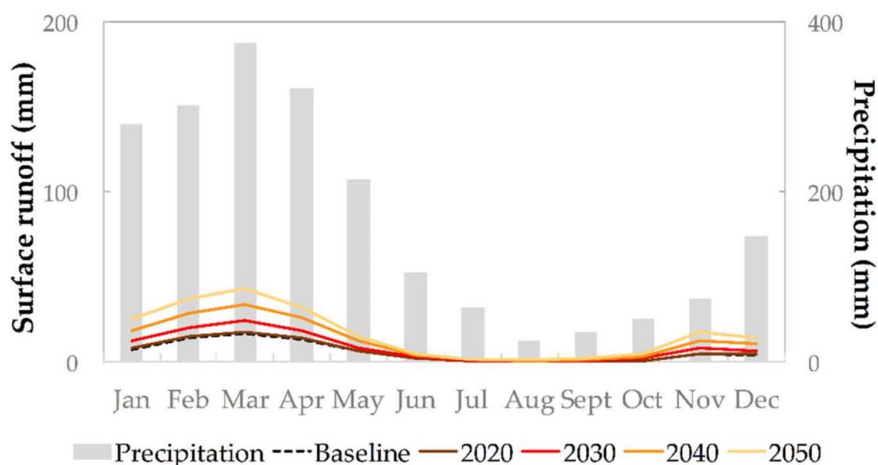

Figure 8. Monthly average simulated surface runoff for 2020, 2030, 2040, 2050, and the baseline.

Calculated on an annual average basis, Perc decreased from −0.1% to −21.9% between 2020 and 2050 (Table 4). The monthly Perc dynamics depended on precipitation (Figure 9). Perc remained negligible in the dry season, from July to October (<5 mm/month). From November to December, Perc increased slightly with deforestation compared to the baseline. Inversely, from January to June, Perc was strongly reduced. Perc is controlled by ET and infiltration capacity. Considering the soils and the climate of the Iriri River basin, the actual ET was significantly reduced from November to December (Figure 7) and as the soil infiltration capacity was not saturated, Perc increased slightly. From January to June, actual ET was weakly reduced and the soil infiltration capacity in pasture was saturated by higher precipitation.
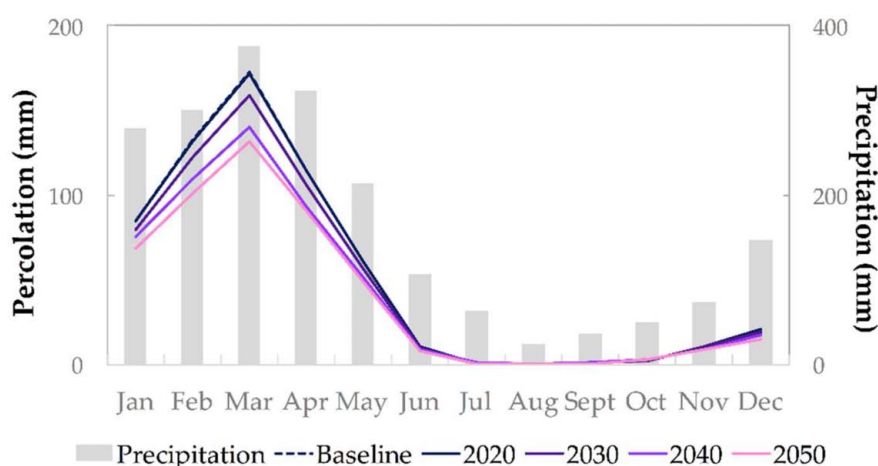

Figure 9. Monthly average simulated percolation for 2020, 2030, 2040, 2050, and the baseline.

5. Discussion

Based on hydrological modelling, our study shows that changes in land cover significantly affect streamflow (Q) and water balance components (WBC) in a tropical basin. Calculated on an annual

average basis, these results are in accordance with those of other studies showing that deforestation increases Q [10,24,78,87,88,90–92]. In the Xingu River Basin, Panday et al. [78] found that deforestation of 15% of the basin over a period of 30 years caused a 6% increase in annual Q. Also in the Xingu River Basin, Cristina et al. [87] highlighted a greater impact of deforestation; at the scale of completely deforested and cropped small catchments, the measured mean Q in soy catchments was three times greater than that of forest catchments.

Concerning the impact of land use change (LUC) on WBC, previous studies have reported that a reduction of forested areas reduces evapotranspiration (ET) from both canopy interception and plant transpiration and simultaneously increases surface runoff (SurfQ) and Q, particularly during the rainy season [78,87]. The deep roots of the trees enable them to tap the water stored in deep soil layers and to maintain a high ET rate during the dry season [9,42,45–47,93]. In contrast, even in wet equatorial areas, pastures converted to forest are subject to a decline in photosynthetic activity in the dry season as a consequence of increasing water stress [46,47]. The greater sensitivity of pasture to drought than primary forest can be explained by grass phenology and shallower roots; these roots, which have less access to deep soil water, reduces the ET. Consequently, the water stored in the deep soil is less depleted in pastureland and Q begins to rise earlier.

When forest is transformed into pasture, soil compaction due to trampling cattle as well as reduced vegetation cover and organic matter, reduce infiltration capacity and increase the Horton overland flow in pastures compared with forest [88,89,94–96]. In small catchments of the Upper Xingu River Basin, on Oxisols, Scheffler et al. [97] measured a reduction in infiltration from 1258 mm/h to 100 mm/h after conversion of forest into pasture. Consequently, a larger fraction of precipitation is transformed into SurfQ thereby reducing the vertical flow path caused by infiltration, as shown in our results on Percolation (Perc) (Figure 9). The groundwater reserves are thus insufficiently replenished in the rainy season and there is a major decline in Q at the beginning of the dry season, as measured by Bruijnzeel [98], which is in agreement with the lower Q simulated between April and June in the Iriri River basin (Figure 6). These results are in accordance with those of Bruijnzeel [99], who found an increase in baseflow and reduced ET after deforestation when the surface infiltration characteristics were maintained as well as a reduced baseflow when infiltration was strongly impaired. Inversely, Bruijnzeel's [99] results showed an increase in Q from low water to peak flow (July to February), a lower ET, and a higher SurfQ. Modelling the replacement of forest by pasture in large savanna basins in the Amazon, Lamparter et al. [11] also found an increase in monthly Q at the beginning of the rainy season. These authors explained the increase during this period by a reduced ET and an increased SurfQ. However, in the present study, modelling the impacts of LUC did not lead to higher peak Q in contrast to the results reported by other studies [10,98,100,101].

Our model did not include climate feedback such as reduced precipitation caused by deforestation nor global climate change. Previous studies [10,23,24] analyzed the climate–vegetation balance in the Amazon region; extensive deforestation affects atmospheric dynamics, leading to a reduction in precipitation and consequently an increase in the duration and intensity of the dry season in the Amazon basin with major changes in WBC. The increased water yield simulated by our model may be partially or fully offset by reduced precipitation with complex non-linear relationships between deforestation and Q. After modeling recent decades in the Xingu River basin, Panday et al. [78] suggested that climate variations led to a decrease in the annual average Q as a result of a decrease in precipitation and an increase in ET; this was partially offset by the increase caused by deforestation. The simulations they performed, from the 1970s to the 2000s, suggested that climate variations alone accounted for a −14% decrease in annual discharge while deforestation alone caused a +6% increase in annual discharge. Thus, climate feedback may compensate land use change effects on the Iriri basin.

The results shown here depend on the design and assumptions of the SWAT model and represent one example of an application of this model in the Amazon region. Although the SWAT model was originally developed for temperate zones and that some input data and the method require certain improvements before it can be applied in tropical regions [39–41], there has been an increase in its

application in tropical zones in recent years. Many of these studies reported that the model performed well for simulated Q and/or water quality (model calibration and validation is usually based on these parameters), but these results do not say which hydrological processes, such as ET, SurfQ, and Perc, were simulated correctly [40]. Our calibration results represented a good performance (calibration based on monthly Q data) and the simulated ET (calibration based on yearly data) matched ET rates measured or estimated for the region [44,47,77,78] as well as showed a decrease during the dry season correlated with water stress. However, this result contradicts the observational syntheses of Shuttleworth [102], who showed that during the first months of the dry season, ET was not lower than the wet season in the Amazon rain forest. More recent studies have drawn the same conclusions [44,46,47]: water stored in the soil that is available for root uptake is sufficient to maintain the ET rate. But independent of monthly ET results, our findings strongly support the likelihood that deforestation will have serious consequences for WBC in a large basin in the Amazonian region.

6. Conclusions

In this study, we used the SWAT model to investigate the hydrologic response to land use change (LUC) in a large river basin in the eastern Amazon. The LUC involved progressive deforestation (between 2020 and 2050), from >8 to <57%, in the Iriri River basin. The results of this study point to the serious potential consequences of deforestation on monthly streamflow and water balance components in an Amazonian basin. A ~6% decrease in the forested area (2020) would lead to a negligible increase in streamflow (0.3%); however, a ~57% change in land cover from forest to pasture (2050) would cause a ~6.5% increase in streamflow as well as higher surface runoff, less percolation, and evapotranspiration compared to the baseline scenario.

Today, about 80% of the Iriri River basin is legally protected area. Our findings emphasize the importance of protected areas for conservation strategies in the Brazilian Amazonian region; these include maintaining the climate–vegetation balance and hydrological regimes, preventing forest fires, as well as sustaining traditional livelihoods and "green barriers" to deforestation [6,8]. The insights acquired in this study provide further evidence of and useful references for the importance of regional land use and water resources planning in the Amazon basin.

Author Contributions: Vanessa Dos Santos collected the input data for the model, performed the modelling work and analysis, and wrote the manuscript; François Laurent proposed the methodology for the study and wrote the manuscript; Camila Abe collected the input data for the model, conducted the analysis, and revised the manuscript; François Messner collected the input data for the model.

Conflicts of Interest: The authors declare no conflict of interest.

References

1. Coe, M.T.; Macedo, M.N.; Brando, P.M.; Lefebvre, P.; Panday, P.; Silvério, D. The Hydrology and Energy Balance of the Amazon Basin. In *Interactions between Biosphere, Atmosphere and Human Land Use in the Amazon Basin*; Nagy, L., Forsberg, B.R., Artaxo, P., Eds.; Springer: Berlin/Heidelberg, Germany, 2016; pp. 34–53, ISBN 978-3-662-49902-3.
2. Martini, D.Z.; Moreira, M.A.; Cruz de Aragão, L.E.O.E.; Formaggio, A.R.; Dalla-Nora, E.L. Potential land availability for agricultural expansion in the Brazilian Amazon. *Land Use Policy* **2015**, *49*, 35–42. [CrossRef]
3. Soares-Filho, B.; Rajão, R.; Macedo, M.; Carneiro, A.; Costa, W.; Coe, M.; Rodrigues, H.; Alencar, A. Cracking Brazil's Forest Code. *Science* **2014**, *344*, 363–364. [CrossRef] [PubMed]
4. Nepstad, D.; McGrath, D.; Stickler, C.; Alencar, A.; Azevedo, A.; Swette, B.; Bezerra, T.; DiGiano, M.; Shimada, J.; Da Motta, R.S.; et al. Slowing Amazon deforestation through public policy and interventions in beef and soy supply chains. *Science* **2014**, *344*, 1118–1123. [CrossRef] [PubMed]

5.   Hilker, T.; Lyapustin, A.I.; Tucker, C.J.; Hall, F.G.; Myneni, R.B.; Wang, Y.; Bi, J.; Mendes de Moura, Y.; Sellers, P.J. Vegetation dynamics and rainfall sensitivity of the Amazon. *Proc. Natl. Acad. Sci. USA* **2014**, *111*, 16041–16046. [CrossRef] [PubMed]

6.   Soares-Filho, B.; Moutinho, P.; Nepstad, D.; Anderson, A.; Rodrigues, H.; Garcia, R.; Dietzsch, L.; Merry, F.; Bowman, M.; Hissa, L.; et al. Role of Brazilian Amazon protected areas in climate change mitigation. *Proc. Natl. Acad. Sci. USA* **2010**, *107*, 10821–10826. [CrossRef] [PubMed]

7.   Malhi, Y.; Roberts, J.T.; Betts, R.A.; Killeen, T.J.; Li, W.; Nobre, C.A. Climate change, deforestation, and the fate of the Amazon. *Science* **2008**, *319*, 169–172. [CrossRef] [PubMed]

8.   Soares-Filho, B.S.; Nepstad, D.C.; Curran, L.M.; Cerqueira, G.C.; Garcia, R.A.; Ramos, C.A.; Voll, E.; McDonald, A.; Lefebvre, P.; Schlesinger, P. Modelling conservation in the Amazon basin. *Nature* **2006**, *440*, 520–523. [CrossRef] [PubMed]

9.   Nepstad, D.C.; de Carvalho, C.R.; Davidson, E.A.; Jipp, P.H.; Lefebvre, P.A.; Negreiros, G.H.; da Silva, E.D.; Stone, T.A.; Trumbore, S.E.; Vieira, S. The role of deeps roots in the hydrological and carbon cycles of Amazonian forests and pastures. *Nature* **1994**, *372*, 666–669. [CrossRef]

10.   D'Almeida, C.; Vörösmarty, C.J.; Hurtt, G.C.; Marengo, J.A.; Dingman, S.L.; Keim, B.D. The effects of deforestation on the hydrological cycle in Amazonia: A review on scale and resolution. *Int. J. Climatol.* **2007**, *27*, 633–647. [CrossRef]

11.   Lamparter, G.; Nobrega, R.L.B.; Kovacs, K.; Amorim, R.S.; Gerold, G. Modelling hydrological impacts of agricultural expansion in two macro-catchments in Southern Amazonia, Brazil. *Reg. Environ. Chang.* **2016**, 1–13. [CrossRef]

12.   Brown, D.S.; Brown, J.C.; Brown, C. Land occupations and deforestation in the Brazilian Amazon. *Land Use Policy* **2016**, *54*, 331–338. [CrossRef]

13.   Rivero, S.; Almeida, O.; Ávila, S.; Oliveira, W. Pecuária e desmatamento: Uma análise das principais causas diretas do desmatamento na Amazônia. *Nov. Econ.* **2009**, *19*, 41–66. [CrossRef]

14.   Fearnside, P.M. Desmatamento na Amazônia: Dinâmica, impactos e controle. *Acta Amaz.* **2006**, *36*, 395–400. [CrossRef]

15.   Laurent, F.; Arvor, D.; Daugeard, M.; Osis, R.; Tritsch, I.; Coudel, E.; Piketty, M.-G.; Piraux, M.; Viana, C.; Dubreuil, V.; et al. Le tournant environnemental en Amazonie: Ampleur et limites du découplage entre production et déforestation. *EchoGéo* **2017**, *41*, 1–27. [CrossRef]

16.   Instituto Nacional de Pesquisas Espaciais (INPE). PROJETO PRODES DIGITAL: Mapeamento do desmatamento da Amazônia com Imagens de Satélite. Available online: http://www.obt.inpe.br/prodes/index.php (accessed on 22 February 2017).

17.   Refsgaard, J.C.; Abbott, M.B. The role of distributed hydrological modelling in water resources management. In *Distributed Hydrological Modelling*; Abbott, M.B., Refsgaard, J.C., Eds.; Kluwer Academic Publishers: Dordrecht, The Netherlands, 1996; Volume 22, 336p, ISBN 0-7923-4042-6.

18.   Abbaspour, K.C.; Rouholahnejad, E.; Vaghefi, S.; Srinivasan, R.; Yang, H.; Kløve, B. A continental-scale hydrology and water quality model for Europe: Calibration and uncertainty of a high-resolution large-scale SWAT model. *J. Hydrol.* **2015**, *524*, 733–752. [CrossRef]

19.   Loucks, D.P.; van Beek, E.; Stedinger, J.R.; Dijkman, J.P.M.; Villars, M.T. *Water Resources Systems Planning and Management and Applications: An Introduction to Methods, Models and Applications*; United Nations Educational (UNESCO): Bangalore, India, 2005; pp. 39–56, ISBN 92-3-103998-9.

20.   Woldesenbet, T.A.; Elagib, N.A.; Ribbe, L.; Heinrich, J. Hydrological responses to land use/cover changes in the source region of the Upper Blue Nile Basin, Ethiopia. *Sci. Total Environ.* **2017**, *575*, 724–741. [CrossRef] [PubMed]

21.   Kamali, B.; Kouchi, D.H.; Yang, H.; Abbaspour, K.C. Multilevel drought hazard assessment under climate change scenarios in semi-arid regions-a case study of the karkheh river basin in Iran. *Water* **2017**, *9*, 214. [CrossRef]

22.   Zhang, Y.; Zhao, Y.; Wang, Q.; Wang, J.; Li, H.; Zhai, J.; Zhu, Y.; Li, J. Impact of land use on frequency of floods in Yongding River Basin, China. *Water* **2016**, *8*, 401. [CrossRef]

23.   Lima, L.S.; Coe, M.T.; Soares Filho, B.S.; Cuadra, S.V.; Dias, L.C.P.; Costa, M.H.; Lima, L.S.; Rodrigues, H.O. Feedbacks between deforestation, climate, and hydrology in the Southwestern Amazon: Implications for the provision of ecosystem services. *Landsc. Ecol.* **2014**, *29*, 261–274. [CrossRef]

24. Coe, M.T.; Costa, M.H.; Soares-Filho, B.S. The influence of historical and potential future deforestation on the stream flow of the Amazon River—Land surface processes and atmospheric feedbacks. *J. Hydrol.* **2009**, *369*, 165–174. [CrossRef]

25. Arnold, J.G.; Srinivasan, R.; Muttiah, R.S.; Williams, J.R. Large area hydrologic modeling and assesment Part I: Model development. *J. Am. Water Resour. Assoc.* **1998**, *34*, 73–89. [CrossRef]

26. Gassman, P.P.W.; Reyes, M.M.R.; Green, C.C.H.; Arnold, J.J.G. The Soil and Water Assessment Tool: Historical development, applications, and future research directions. *Trans. ASAE* **2007**, *50*, 1211–1250. [CrossRef]

27. Neitsch, S.; Arnold, J.; Kiniry, J.; Williams, J. *Soil and Water Assessment Tool*; Theoretical Documentation: Version 2009; Texas Water Resources Institute: College Station, TX, USA, 2011.

28. Silva, J.D.P. Avaliação da diversidade de padrões de canais fluviais e da geodiversidade na Amazônia—Aplicação e discussão na Bacia Hidrografica do Rio Xingu. Ph.D. Thesis, Universidade de São Paulo, São Paulo, Brazil, 2012.

29. Lucas, E.W.M.; Assis, F.D.E.; Sousa, S.D.E.; Daniel, F.; Santos, D.O.S.; Lucio, P.S. Modelagem hidrológica determinística e estocástica aplicada à região hidrográfica do Xingu—Pará. *Rev. Bras. Meteorol.* **2009**, *24*, 308–322. [CrossRef]

30. Centrais Eleétricas Brasileiras S.A. (Eletrobras). AAI—Avaliação Ambiental Integrada dos aproveitamentos hidroelétricos da bacia do rio Xingu. Available online: http://eletrobras.com/pt/AreasdeAtuacao/geracao/belo_monte/AAI-Xingu-Volume-I.pdf (accessed on 24 November 2016).

31. De Almeida, C.A.; Coutinho, A.C.; César, J.; Mora, D.; Adami, M.; Venturieri, A.; Diniz, C.G.; Dessay, N.; Durieux, L.; Gomes, A.R. High spatial resolution land use and land cover mapping of the Brazilian Legal Amazon in 2008 using Landsat-5/TM and MODIS data. *Acta Amaz.* **2016**, *46*, 291–302. [CrossRef]

32. Villas-Boas, A. *De olho na Bacia do Xingu*; Instituto Socioambiental: São Paulo, Brazil, 2012; ISBN 978-85-85994-97.

33. Arnold, J.G.; Allen, P.M.; Volk, M.; Williams, J.R.; Bosch, D.D. Assessment of Different Representations of Spatial Variability on SWAT Model Performance. *Trans. ASABE* **2010**, *53*, 1433–1443. [CrossRef]

34. United States Geological Survey (USGS). Shuttle Radar Topography Mission (SRTM). Available online: https://earthexplorer.usgs.gov/ (accessed on 26 November 2016).

35. Brazilian National Institute of Meteorology (INMET). Banco de Dados Meteorológicos para Ensino e Pesquisa. Available online: http://www.inmet.gov.br/portal/index.php?r=bdmep/bdmep (accessed on 13 December 2016).

36. National Aeronautics and Space Agency (NASA). TRMM 3B42 Daily v.7 Product. Available online: https://disc.sci.gsfc.nasa.gov/SSW/#keywords= (accessed on 15 December 2016).

37. European Centre for Medium-Range Weather Forecasts (ECMWF). Era Interim Daily Database. Available online: http://apps.ecmwf.int/datasets/data/interim-full-daily/levtype=sfc/ (accessed on 26 February 2017).

38. Brasilian Institute of Geography and Statistics (IBGE). Mapa pedológico da Amazonia Legal 1:250.000. Available online: ftp://geoftp.ibge.gov.br/informacoes_ambientais/pedologia/vetores/escala_250_mil/amazonia_legal/ (accessed on 24 November 2016).

39. Wagner, P.D.; Kumar, S.; Fiener, P.; Schneider, K. Technical Note: Hydrological Modeling with SWAT in a Monsoon-Driven Environment: Experience from the Western Ghats, India. *Trans. ASABE* **2011**, *54*, 1783–1790. [CrossRef]

40. Strauch, M.; Volk, M. SWAT plant growth modification for improved modeling of perennial vegetation in the tropics. *Ecol. Model.* **2013**, *269*, 98–112. [CrossRef]

41. Alemayehu, T.; Van Griensven, A.; Woldegiorgis, B.T.; Bauwens, W. An improved SWAT vegetation growth module and its evaluation for four tropical ecosystems. *Hydrol. Earth Syst. Sci.* **2017**, *21*, 4449–4467. [CrossRef]

42. Wagner, F.H.; Hérault, B.; Rossi, V.; Hilker, T.; Maeda, E.E.; Sanchez, A.; Lyapustin, A.I.; Galvão, L.S.; Wang, Y.; Aragão, L.E.O.C. Climate drivers of the Amazon forest greening. *PLoS ONE* **2017**, *12*, 0180932. [CrossRef] [PubMed]

43. Tang, H.; Dubayah, R. Light-driven growth in Amazon evergreen forests explained by seasonal variations of vertical canopy structure. *Proc. Natl. Acad. Sci. USA* **2017**, *114*, 2640–2644. [CrossRef] [PubMed]

44. Maeda, E.E.; Ma, X.; Wagner, F.; Kim, H.; Oki, T.; Eamus, D. Evapotranspiration seasonality across the Amazon basin Evapotranspiration seasonality across the Amazon basin. *Earth Syst. Dyn.* **2017**, *8*, 439. [CrossRef]

45. Kleidon, A.; Heimann, M. Assessing the role of deep rooted vegetation in the climate system with model simulations: Mechanism, comparison to observations and implications for Amazonian deforestation. *Clim. Dyn.* **2000**, *16*, 183–199. [CrossRef]

46. Huete, A.R.; Didan, K.; Shimabukuro, Y.E.; Ratana, P.; Saleska, S.R.; Hutyra, L.R.; Yang, W.; Nemani, R.R.; Myneni, R. Amazon rainforests green-up with sunlight in dry season. *Geophys. Res. Lett.* **2006**, *33*, 2–5. [CrossRef]

47. Negrón Juárez, R.I.; Hodnett, M.G.; Fu, R.; Gouden, M.L.; von Randow, C. Control of dry season evapotranspiration over the Amazonian forest as inferred from observation at a Southern Amazon forest site. *J. Clim.* **2007**, *20*, 2827–2839. [CrossRef]

48. Huete, A.R.; Ferreira, L.G.; Miura, T. LBA-ECO LC-19 Soil and Vegetation Data for Cerrado and Forested Sites, Brazil: 2002. *ORNL DAAC* **2014**. [CrossRef]

49. Asner, G.P.; Olander, L.P. LBA-ECO LC-21 Foliar Nutrients, Logged Areas, Tapajos Forest, Para, Brazil: 2003. *ORNL DAAC* **2014**. [CrossRef]

50. Brondizio, E.S.; Batistella, M.; Moran, E.F. LBA-ECO LC-09 Vegetation Composition and Structure in the Brazilian Amazon: 1992–1995. *ORNL DAAC* **2009**. [CrossRef]

51. Tomasella, J.; Hodnett, M. Pedotransfer functions for tropical soils. *Dev. Soil Sci.* **2004**, *30*, 415–429. [CrossRef]

52. Quesada, C.A.; Lloyd, J.; Anderson, L.O.; Fyllas, N.M.; Schwarz, M.; Czimczik, C.I. Soils of Amazonia with particular reference to the RAINFOR sites. *Biogeosciences* **2011**, *8*, 1415–1440. [CrossRef]

53. Quesada, C.A.; Lloyd, J.; Schwarz, M.; Patiño, S.; Baker, T.R.; Czimczik, C.; Fyllas, N.M.; Martinelli, L.; Nardoto, G.B.; Schmerler, J.; et al. Variations in chemical and physical properties of Amazon forest soils in relation to their genesis. *Biogeosciences* **2010**, *7*, 1515–1541. [CrossRef]

54. Brondizio, E.S.; Moran, E.F. LBA-ECO LC-09 Soil Composition and Structure in the Brazilian Amazon: 1992–1995. *ORNL DAAC* **2009**. [CrossRef]

55. Sartori, A.; Neto, F.L.; Genovez, A.M. Classificação Hidrológica de Solos Brasileiros para a Estimativa da Chuva Excedente com o Método do Serviço de Conservação do Solo dos Estados Unidos Parte 1: Classificação. *Rev. Bras. Recur. Hidr.* **2005**, *10*, 5–18.

56. Brazilian Agricultural Research Corporation (EMBRAPA/FAO). *Caracterização físico hídrica dos principais solos da Amazônia Legal: Volume I—Estado do Pará*; EMBRAPA/FAO: Belém, Brazil, 1991.

57. National Department of Mineral Production. *Projeto RADAM. Folha SA.22 Belém; Geologia, Geomorfologia, Solos, Vegetação, uso Potencial da Terra*; National Department of Mineral Production: Rio de Janeiro, Brazil, 1974.

58. National Department of Mineral Production. *Projeto RADAM. Folha SB.22 Araguaia e Parte da Folha SC.22 Tocantins; Geologia, Geomorfologia, Solos, Vegetação, uso Potencial da Terra*; National Department of Mineral Production: Rio de Janeiro, Brazil, 1974.

59. Barros, H.S.; Fearnside, P.M. Pedo-Transfer Functions for Estimating Soil Bulk Density in Central Amazonia. *Rev. Bras. Ciência do Solo* **2015**, *39*, 397–407. [CrossRef]

60. Barros, A.H.C.; van Lier, Q.d.J. Pedotransfer Functions for Brazilian Soils. In *Application of Soil Physics in Environmental Analyses Measuring, Modelling and Data Integration*; Teixeira, W.G., Ceddia, M.B., Ottoni, M.V., Donnagema, G.K., Eds.; Springer: Berlin/Heidelberg, Germany, 2014; pp. 128–162.

61. Bernoux, M.; Arrouays, D.; Cerri, C.; Volkoff, B.; Jolivet, C. Bulk density of Brazilian Amazon soils related to other soil properties. *Soil Sci. J.* **1998**, *162*, 743–749. [CrossRef]

62. Batjes, N.H. Total carbon and nitrogen in the soils of the world. *Eur. J. Soil Sci.* **1996**, *47*, 151–163. [CrossRef]

63. Winchell, M.; Srinivasan, R.; Di Luzio, M.; Arnold, J.G. *Arcswat Interface for SWAT2012: User's Guide*; Blackland Research Center, Texas AgriLife Research: Temple, TX, USA, 2013.

64. Hargreaves, G.; Hargreaves, G.; Riley, J. Agricultural benefits for Senegal River Basin. *J. Irrig. Drain. Eng.* **1985**, *111*, 113–124. [CrossRef]

65. USDA Soil Conservation Service. *National Engineering Handbook*; Section 4, Hydrology, Chapter 21; USDA Soil Conservation Service: Washington, DC, USA, 1972.

66. Chow, V.T.; Maidment, D.R.; Mays, L.W. *Applied Hydrology*; McGraw-Hill, Inc.: New York, NY, USA, 1988.

67. Pai, N.; Saraswat, D. SWAT2009_LUC: A Tool to Activate the Land Use Change Module in SWAT 2009. *Trans. ASABE* **2011**, *54*, 1649–1658. [CrossRef]

68. Van Griensven, A.; Meixner, T. Methods to quantify and identify the sources of uncertainty for river basin water quality models. *Water Sci. Technol.* **2006**, *53*, 51–59. [CrossRef] [PubMed]

69. Abbaspour, K. *SWAT-CUP: SWAT Calibration and Uncertainty Programs—A User Manual*; Eawag: Duebendorf, Switzerland, 2015; p. 103.

70. Nash, J.E.; Sutcliffe, J. River flow forecasting through conceptual models: Part 1. A discussion of principles. *J. Hydrol.* **1979**, *10*, 282–290. [CrossRef]

71. Van Griensven, A.; Meixner, T. A global and efficient multi-objective auto-calibration and uncertainty estimation method for water quality catchment models. *J. Hydroinform.* **2007**, *9*, 277. [CrossRef]

72. Gupta, H.V.; Sorooshian, S.; Yapo, P. Status of automatic calibration for hydrologic models: Comparison with multilevel expert calibration. *J. Hydrol. Eng.* **1999**, *4*, 135–143. [CrossRef]

73. Singh, J.; Knapp, H.V.; Arnold, J.G.; Demissie, M. Hydrological modelling of the Iroquois River watershed using HSPF and SWAT. *J. Am. Water Resour. Assoc.* **2005**, *41*, 343–360. [CrossRef]

74. Soares-Filho, B.S.; Nepstad, D.C.; Curran, L.M.; Voll, E.; Cerqueira, G.C.; Garcia, R.A.; Ramos, C.A.; McDonald, A.; Lefebvre, P.; Schlesinger, P. LBA-ECO LC-14 Modeled Deforestation Scenarios, Amazon Basin: 2002–2050. *ORNL DAAC* **2013**. [CrossRef]

75. Bi, J.; Knyazikhin, Y.; Choi, S.; Park, T.; Barichivich, J.; Ciais, P.; Fu, R.; Ganguly, S.; Hall, F.; Hilker, T.; et al. Sunlight mediated seasonality in canopy structure and photosynthetic activity of Amazonian rainforests. *Environ. Res. Lett.* **2015**, *10*, 64014. [CrossRef]

76. Malhado, A.C.M.; Costa, M.H.; de Lima, F.Z.; Portilho, K.C.; Figueiredo, D.N. Seasonal leaf dynamics in an Amazonian tropical forest. *For. Ecol. Manag.* **2009**, *258*, 1161–1165. [CrossRef]

77. Tomasella, J.; Hodnett, M.G.; Cuartas, L.A.; Nobre, A.D.; Waterloo, M.J.; Oliveira, S.M. The water balance of an Amazonian micro-catchment: The effect of interannual variability of rainfall on hydrological behaviour. *Hydrol. Process.* **2008**, *22*, 2133–2147. [CrossRef]

78. Panday, P.K.; Coe, M.T.; Macedo, M.N.; Lefebvre, P.; Castanho, A.D.d.A. Deforestation offsets water balance changes due to climate variability in the Xingu River in eastern Amazonia. *J. Hydrol.* **2015**, *523*, 822–829. [CrossRef]

79. Ellison, D.; Morris, C.E.; Locatelli, B.; Sheil, D.; Cohen, J.; Murdiyarso, D.; Gutierrez, V.; van Noordwijk, M.; Creed, I.F.; Pokorny, J.; et al. Trees, forests and water: Cool insights for a hot world. *Glob. Environ. Chang.* **2017**, *43*, 51–61. [CrossRef]

80. Simmons, L.A.; Anderson, S.H. Effects of logging activities on selected soil physical and hydraulic properties for a claypan landscape. *Geoderma* **2016**, *269*, 145–152. [CrossRef]

81. Food and Agriculture Organization of the United Nations (FAO). *Forests and Water: A Thematic Study Prepared in the Framework of the Global Forest Resources Assessment 2005*; FAO: Rome, Italy, 2008.

82. Chow, V.T. *Open-Channel Hydraulics*; McGraw-Hill, Inc.: New York, NY, USA, 1959.

83. Lane, L.J. Transmission losses. In *SCS National Enginnering Handbook Section 4, Hydrology*; Soil Conservation Service, U.S. Department of Agriculture: Washington, DC, USA, 1983; pp. 19:1–9.21.

84. Hoorn, C.; Roddaz, M.; Dino, R.; Soares, E.; Uba, C. The Amazonian Craton and its influence on past fluvial systems (Mesozoic-Cenozoic, Amazonia). In *Amazonia: Landscape and Species Evolution*; Hoorn, C., Wesselingh, F.P., Eds.; Blackwell Publishing Ltd.: Hoboken, NJ, USA, 2009; pp. 103–122, ISBN 978-1-4051-8113-6.

85. Schneider, R. *Groundwater Provinces of Brazil*; Prepared in Cooperation with the Government of Brazil and the United States Operation Mission to Brazil; United States Government Publishing Office: Washington, DC, USA, 1963.

86. Moriasi, D.N.; Arnold, J.G.; Van Liew, M.W.; Bingner, R.L.; Harmel, R.D.; Veith, T.L. Model Evaluation Guidelines for Systematic Quantification of Accuracy in Watershed Simulations. *Trans. ASABE* **2007**, *50*, 885–900. [CrossRef]

87. Cristina, L.; Dias, P.; Macedo, M.N.; Heil, M.; Coe, M.T.; Neill, C. Effects of land cover change on evapotranspiration and streamflow of small catchments in the Upper Xingu River Basin, Central Brazil. *J. Hydrol. Reg. Stud.* **2015**, *4*, 108–122. [CrossRef]

88. Biggs, T.W.; Dunne, T.; Muraoka, T. Transport of water, solutes and nutrients from a pasture hillslope, southwestern Brazilian Amazon. *Hydrol. Process.* **2006**, *20*, 2527–2547. [CrossRef]

89. De Moraes, J.; Schuler, A.E.; Dunne, T.; Figueiredo, R.O.; Victoria, R.L. Water storage and runoff processes in plinthic soils under forest and pasture in Eastern Amazonia. *Hydrol. Process.* **2006**, *20*, 2509–2526. [CrossRef]

90. Bosch, J.M.; Hewlett, J.D. A review of catchment experiments to determine the effect of vegetation changes on water yield and evapotranspiration. *J. Hydrol.* **1982**, *55*, 3–23. [CrossRef]

91. Davidson, E.A.; De Araüjo, A.C.; Artaxo, P.; Balch, J.K.; Brown, I.F.; Mercedes, M.M.; Coe, M.T.; Defries, R.S.; Keller, M.; Longo, M.; et al. The Amazon basin in transition. *Nature* **2012**, *481*, 321–328. [CrossRef] [PubMed]

92. Hayhoe, S.J.; Neill, C.; Porder, S.; Mchorney, R.; Lefebvre, P.; Coe, M.T.; Elsenbeer, H.; Krusche, A.V. Conversion to soy on the Amazonian agricultural frontier increases streamflow without affecting stormflow dynamics. *Glob. Chang. Biol.* **2011**, *17*, 1821–1833. [CrossRef]

93. Fan, Y.; Miguez-Macho, G. Potential groundwater contribution to Amazon evapotranspiration. *Hydrol. Earth Syst. Sci.* **2010**, *14*, 2039–2056. [CrossRef]

94. Chaves, J.; Neill, C.; Germer, S.; Gouveia Neto, S.; Krusche, A.; Elsenbeer, H. Land management impacts on runoff sources in small Amazon watersheds. *Hydrol. Process.* **2008**, *22*, 1766–1775. [CrossRef]

95. Zimmermann, B.; Elsenbeer, H.; De Moraes, J.M. The influence of land-use changes on soil hydraulic properties: Implications for runoff generation. *For. Ecol. Manag.* **2006**, *222*, 29–38. [CrossRef]

96. Martínez, L.J.; Zinck, J.A. Temporal variation of soil compaction and deterioration of soil quality in pasture areas of Colombian Amazonia. *Soil Tillage Res.* **2004**, *75*, 3–17. [CrossRef]

97. Scheffler, R.; Neill, C.; Krusche, A.V.; Elsenbeer, H. Soil hydraulic response to land-use change associated with the recent soybean expansion at the Amazon agricultural frontier. *Agric. Ecosyst. Environ.* **2011**, *144*, 281–289. [CrossRef]

98. Bruijnzeel, L.A. Hydrological functions of tropical forests: Not seeing the soil for the trees? *Agric. Ecosyst. Environ.* **2004**, *104*, 185–228. [CrossRef]

99. Bruijnzeel, L.A. (De)forestation and dry season flow in the tropics: A closer look. *J. Trop. For. Sci.* **1989**, *1*, 229–243.

100. Brown, A.E.; Zhang, L.; McMahon, T.A.; Western, A.W.; Vertessy, R.A. A review of paired catchment studies for determining changes in water yield resulting from alterations in vegetation. *J. Hydrol.* **2005**, *310*, 28–61. [CrossRef]

101. Rodrigues, A.S.L.; Ewers, R.M.; Parry, L.; Souza, C.; Veríssimo, A.; Balmford, A. Boom-and-bust development patterns across the amazon deforestation frontier. *Science* **2009**, *324*, 1435–1437. [CrossRef] [PubMed]

102. Shuttleworth, W.J. Evaporation from Amazonian Rainforest. *Proc. R. Soc. B Biol. Sci.* **1988**, *233*, 321–346. [CrossRef]